Polyanionic and octet phases in the K-Sb system. I. Crystalline intermetallic compounds

K. Seifert-Lorenz and J. Hafner
Institut für Theoretische Physik and Center for Computational Material Science, Technische Universität Wien, Wiedner Hauptstraße 8/10, A-1040 Wien, Austria
(Received 29 June 1998)

The crystal structure, chemical bonding, and electronic properties of intermetallic compounds in the K-Sb system have been investigated using first-principle–local-density-functional calculations including generalized gradient corrections. It is shown that the chemical bonding obeys a generalized Zintl principle, i.e., a formally complete electron transfer from K to Sb. The stable crystal structure is determined for the stoichiometric octet compound K_3Sb by the formation of an ionic lattice and at the equiatomic composition by the formation of covalently bonded Sb_∞^- helices in close analogy to the isoelectronic chalcogen elements. At intermediate compositions the Sb atoms cluster together to form chainlike polyanion radicals, the electrons provided by the excess alkali metal serving to partially saturate the dangling bonds at the chain ends. It is demonstrated that density-functional theory describes the crystal structure of all compounds with high accuracy. The overbinding characteristic of the local-density approximation is most pronounced in the alkali-rich limit, but merely causes a scaling of all interatomic distances without distorting the structure. Gradient corrections substantially improve the prediction at large K content, but tend to overshoot in the Sb-rich range. [S0163-1829(99)01102-9]

I. INTRODUCTION

Alloys of the alkali or alkaline-earth metals with elements from the post-transition-metal groups III to VI have been in the center of intense research efforts for many decades because of their outstanding structural, electronic, and thermodynamic properties that are at the borderline between metals, semiconductors, and salts.[1] The picture originally proposed by Zintl and co-workers[2,3] and Hückel[4] suggests that the driving force behind the interesting physicochemical properties is ionicity: Because of the large difference in the electronegativities the alkali or alkaline-earth atoms transfer their valence electrons to the more electronegative polyvalent element. At a composition where the charge transfer completes the octet shell of the polyvalent element, this leads to the formation of saltlike compounds like K_3Sb crystallizing in the Bi_3F structure. In accordance with the band-filling model for the metal-nonmetal transition, the octet compounds are narrow-gap semiconductors. At a lower concentration of the alkali metal the charge transferred is not sufficient to complete the octet shell. A saturated chemical bond between the polyvalent atoms can be achieved only by sharing valence electrons among the anions, leading to the formation of polyanion cluster compounds. In the I-VI alloys the polyanions are pairs of chalcogen ions, isoelectronic to halogen molecules, e.g., Te_2^{-2} dimers identified in K_2Te_2 isostructural with Li_2O_2 (Refs. 5–7). The polyanionic cluster compound K_2Te_2 coexists with the octet compound K_2Te. In the I-V alloys the anions (e.g., Sb^-) are isoelectronic to the chalcogen atoms (e.g., Se) and according to the Zintl principle the anions cluster together to form spiral chains similar to those formed in the crystal structures of the chalcogen elements. Classical examples are the alkali antimonides, arsenides, and phosphides crystallizing in the LiAs and NaP structures.[8–10] Octet and polyanionic compounds are known to coexist in many alkali-antimonides and arsenides. In the I-IV alloys the anions (e.g., Sn^-) are isoelectronic to the pentavalent atoms that are known to form tetrahedral molecules in the gas phase. By analogy the Sn^- or Pb^- anions cluster to form covalently bonded tetrahedral Sn_4^{4-} or Pb_4^{4-} polyanions.[11] Finally, in the I-III alloys the anions (e.g., Al^-) are isoelectronic to the tetravalent elements (e.g., Si) and the ''polyanions'' are now infinite sublattices, e.g., the diamondlike sublattice of the Al^- ions in the NaTl-type LiAl—this is even the classical example of a ''Zintl compound.''[2]

The Zintl picture requires the formal transfer of *all* valence electrons from the electropositive to the more electronegative atom. The fact that early electronic structure calculations indicated that the real charge transfer [determined, e.g., by integrating the charges within the atomic spheres or from LCAO (linear combinations of atomic orbitals) projections of the valence states] is small has lead to a widespread critique of the Zintl model.[12–14] It has now become clear that charge transfer (a quantity that is notoriously difficult to define and to determine in a quantitative way) is not the distinguishing feature of Zintl alloys. It is better to say that their valence-electron states are governed by the strongly attractive electron-ion potential of the more electronegative element.

(1) In I-III alloys the valence states form more or less perfect sp^3 hybrids as in the tetrahedral semiconductors.[15–17]

(2) In equiatomic I-IV alloys the valence bonds may be indexed according to the irreducible representations of the tetrahedron group (i.e., they correspond closely to the broadened energy levels of P_4 or As_4 molecules[18–20]) while the octet or near-octet compounds (e.g., $Na_{15}Pb_4$, Li_7Pb_2) are characterized by an ionic gap separating the highest occupied anion state from the lowest empty cation state.

(3) For the I-V alloys an ionic band structure is now firmly established for the 3:1 octet compounds.[16,21,22] For the equiatomic compound the upper valence band has been shown to be characterized by the same tripartite bonding, nonbonding, and antibonding structure (with the Fermi level in the narrow gap between the nonbonding and antibonding

bands) that is also the distinguishing feature of the chalcogen elements.[23,24]

Within the last decade renewed interest in the chemical bonding of Zintl phases has been stimulated by the discovery that the bond has considerable stability and flexibility.

(1) The high-temperature phases of CsPb and NaSn (both contain tetrahedral polyanions) are plastic crystals, in this case ''rotor phases'' in which the polyanions rotate rather freely within the crystal.[25,26]

(2) There is considerable evidence from neutron- and x-ray-diffraction experiments that both the saltlike order of the octet phases and the polyanionic clusters are preserved, at least at some degree, on melting (for recent reviews on molten Zintl alloys see, e.g., van der Lugt[27] and Winter[28]).

The high degree of local order is also considered to be responsible for the sharp anomalies at the ''stoichiometric'' composition observed in the electrical transport, optical, and thermodynamic properties of the melt.

However, at present conclusions drawn on the basis of a large number of diffraction experiments,[27,28] computer modeling studies based on the reverse Monte Carlo (RMC) technique,[29] as well as theoretical studies performed at different levels—from studies based on effective pair interactions[17,30] to *ab initio* density-functional molecular dynamics[31–34] (MD)—agree on the existence of a certain fraction of polyanions, but in a much smaller amount and with less perfect structure than the sharpness of certain experimental features (superstructure peaks in the diffraction data, maxima in the electrical resistivities and in the Darken excess stability functions) seems to suggest. A possible answer to this paradox could be that despite a considerable blurring of the polyanionic structure in the fluid phase, the electronic spectrum and hence the chemical bonding and physical properties are comparatively little affected on melting.

Whether this conjecture is realistic can be decided only at the basis of self-consistent calculations of the atomic and the electronic structure of both the solid and liquid phases. All the electronic structure calculations performed so far for crystalline Zintl alloys[12–22] deal only with the electronic spectrum at the experimentally determined atomic geometry and hence do not discuss the problem of the structural stability of Zintl compounds at all [apart from a few calculations of the relative stability of the *B*2 (CsCl-type) and *B*32 (NaTl-type) phases of the I-III compounds[16,15]]. The *ab initio* MD calculations[31–34] on the other hand did not discuss the stability of the crystalline structure.

Our present work is devoted to *ab initio* density-functional calculations of crystalline and liquid Zintl alloys in the K-Sb system at compositions ranging from the octet to the polyanionic cluster phase. The K-Sb system has been selected for our investigations because in addition to the octet phase K_3Sb with the BiF_3 structure and a polyanionic equiatomic phase KSb with the LiAs structure[9] (where the ''polyanions'' are infinite Sb_∞^- chains), the structure of an intermediate K_5Sb_4 phase has been determined.[35] The crystal structure of K_5Sb_4 contains short Sb_4 chains. The existence of such a phase offers the opportunity to study the transition from octet to polyanionic bonding. (We also mention that the solid compounds are of some interest as materials for photoemitters.) In the liquid state, a sharp maximum of the Darken excess stability function has been reported[36] at the octet composition (weaker than in Na_3Sb, but stronger than in Cs_3Sb), and a broader maximum has been found near the equiatomic composition.[37] The anomalies in the stability function correlate with minima in the electrical conductivity: again a well-defined but shallow minimum at the octet composition[38] and a broad plateaulike minimum between 40 and 50 at. % Sb[36] suggest a strong polyanionic bond with considerable flexibility. Neutron-diffraction measurements of the atomic structure of K-Sb have been performed,[39] demonstrating the existence of sharp prepeaks at $Q \sim 1.1$ Å^{-1} in both the octet and equiatomic composition. Previous diffraction experiments on a number of Cs-Sb alloys[40,41] have demonstrated the existence of a sharp prepeak at $Q_p \sim 0.95$ Å^{-1}, corresponding through the rule of thumb $\lambda Q_p \sim 2\pi$ to a superstructure with a characteristic length of $\lambda \sim 7$ Å. Together with the peak in the radial distribution function at ~2.83 Å (which is very close to the intrachain bond length in the crystal) this has been taken as indicator for the existence of broken polyanionic chains in the melt.

In our calculations for both solid and liquid phases the equilibrium atomic structure is determined by a static total-energy minimization and by canonical molecular-dynamics simulations, respectively. The electronic structure of the equilibrium configuration is calculated and the nature of chemical bond is analyzed in terms of partial valence-charge distributions and electron-localization functions. A unifying result of our investigation is that in all crystalline and liquid alloys, the lowest empty cation state lies above the highest occupied anion state. Hence there is always some charge transfer, although due to the extended nature of the cation states ionicities calculated in terms of net ionic charges are small. If we take the electronic structure as the defining feature of a charge-transfer compound, the K-Sb alloys conform with the original Zintl concept. A further characteristic feature of our results is the strong and rather localized covalent Sb-Sb bond in the polyanionic phases. The localized nature of the bonds explains that the characteristic physical properties of the polyanionic phases subsists even if the long-range order disappears on melting.

The presentation of our results is organized as follows: In Sec. II we briefly review the methodological basis of our work and we discuss the influence of gradient corrections on the prediction of the cohesive and structural properties of the pure elements. Section III describes the structural, electronic, and chemical bonding properties of the crystalline octet compounds; Secs. IV and V describe the cluster compounds KSb and K_5Sb_4. The validity of the generalized Zintl picture for the crystalline K-Sb compounds is discussed in Sec. VI. In the following paper,[70] the properties of the corresponding molten alloys will be discussed on the basis of *ab initio* molecular-dynamics simulations.

II. CALCULATION

All our calculations have been performed using the Vienna *ab initio* simulation program VASP.[42–45] VASP is based on the local-density functional approximation for describing electronic exchange and correlation (we use the functional derived from Ceperley and Alder as parametrized by Perdew and Zunger[46]), a plane-wave expansion of the

TABLE I. Calculated equilibrium structure (atomic volume ω, cohesive energy E, axial ratio c/a, internal structure parameter u, ratio d_2/d_1 of intralayer and interlayer distances, bulk modules B) of trigonal Sb and body-centered-cubic K, obtained in the local-density approximation (LDA) and generalized-gradient approximation (GGA).

(a) Trigonal Sb

	Ω (Å^3)	E (eV/atom)	c/a	u	d_2/d_1	B (Mbar)
LDA	29.15	−4.83	2.55	0.2355	1.13	0.42
GGA-PB[a]	33.24	−2.60	2.67	0.230	1.18	0.22
GGA-PW[b]	31.35	−4.16	2.60	0.2341	1.16	0.29
Expt.[c]	29.96		2.60	0.2336	1.15	0.41

(b) Cubic K

	Ω (Å^3)	E (eV/atom)	B (kbar)
LDA	66.59	−1.13	42.5
LDA-3p[d]		−1.12	42.6
GGA[b]	73.96	−1.03	34.0
GGA-3p[b,d]	68.91	−1.03	33.5
Expt.[c]	71.32		36.7

[a]Perdew-Becke functional, Ref. 52.
[b]Perdew-Wang functional, Refs. 51 and 54.
[c]After Refs. 58 and 57.
[d]Treating 3p electrons as valence electrons.

valence states and a description of the electron-ion interaction in terms of optimized ultrasoft pseudopotentials. Fully nonlocal ultrasoft pseudopotentials for both K and Sb were constructed according to the prescription of Vanderbilt[47] as modified by Kresse and Hafner.[48] For Sb, both s and p components were modeled by ultrasoft pseudopotentials with two reference energies, a cutoff radius of $R_{c,s}=R_{c,p}=3.1$ a.u. for the pseudo-wave-functions and a radius of $R_{aug,s}=R_{aug,p}=2.7$ a.u. for constructing the augmentation functions. The d component has been modeled by a norm-conserving pseudopotential with a cutoff radius of $R_{c,d}=3.1$ a.u. The d component was chosen to be the local pseudopotential; the atomic reference configuration was s^2p^3. The pseudopotential has been tested extensively in calculations of the structural and electronic properties of both crystalline[49] and liquid[50] Sb. We note in particular the excellent agreement for the crystalline and liquid structure of Sb with experiment achieved at the level of the local-density approximation.[49,50] If gradient corrections to the exchange-correlation functional[51–54] are used, the calculated equilibrium volume is increased, the bulk modulus is strongly decreased, and the description of the crystal structure is less accurate (see Table I). In particular we note that the difference between the short and the long nearest-neighbor distances (which is the characteristic feature of the arsenic $A6$ structure produced by a Peierls distortion from the simple cubic structure) is increased. The change in the structure is a pure volume effect; at fixed volume the gradient corrections do not affect the crystal structure. Hence for Sb the standard local-density approximation (LDA) is more accurate than the functional in the generalized gradient approximation (GGA).

For K we also use an ultrasoft pseudopotential with cutoff radii $R_{c,s}=R_{c,p}=3.84$ a.u. and $R_{c,d}=3.48$ a.u. As local potential the d component was chosen. The reference configuration was s^1. It is well known that the LDA leads to a poor prediction of the atomic volume of the alkali metals. This is confirmed by our pseudopotential results, which are in excellent agreement with all-electron calculations (see Table I). It has been claimed that for the heavier alkali metals p-type semicore states (3p states in the case of K) must be unfrozen. However, we find that with a pseudopotential treating the 3p states as valence states the prediction of the atomic volume is not improved (Table I). On the other hand, the gradient corrections lead to a very good agreement with experiment.

Hence the proper choice of the exchange-correlation functional for K-Sb alloys is a dilemma: K is better described in the GGA, Sb in the LDA. Because we expect the bonding properties of the alloys to be determined by Sb-Sb bonds (with exception of the octet compound), gradient corrections have been used only for the K-rich octet phase.

The calculation of the electronic ground state is based on an iterative diagonalization of the Kohn-Sham Hamiltonian, based on the minimization of the norm of the residual vector to the occupied eigenstates and some of the unoccupied states and on an optimized charge-density mixing (for details we refer to Refs. 43 and 45). Brillouin-zone integrations have been performed using a grid of special Monkhorst-Pack[55] points together with a modest Methfessel-Paxton[56] smearing of $\sigma=0.1$ eV. For the low-symmetry structures of KSb and K_5Sb_4, the special-point grid was constructed using the symmetry package implemented in VASP. Convergence of the total energy and the forces acting on the atoms with respect to the density of the k-point grid has been carefully tested. For the K_3Sb structure, a $(5\times5\times5)$ was found to produce adequate convergence. Grids of comparable density have been used for the two other compounds.

The equilibrium atomic structure has been calculated by simultaneously relaxing the volume and the shape of the unit cell and all internal structural parameters, subject to the only

TABLE II. Atomic structure and cohesive properties of crystalline BiF_3-type K_3Sb as calculated in the local-density approximation (LDA) and generalized-gradient approximation (GGA), compared to experiment.

Pearson symbol $cF16$, space group $Fm\bar{3}m$				
Atomic positions within the unit cell				
		x	y	z
K1	(4*b*)	0.5	0.5	0.5
K2	(8*c*)	0.25	0.25	0.25
Sb	(4*a*)	0	0	0
		LDA	GGA	Expt.[a]
Atomic volume Ω (Å^3)		35.35	38.92	38.29
Excess volume $\Delta\Omega$ (%)		−38.2	−38.5	−37.2
Lattice parameter a (Å)		8.27	8.54	8.49
Cohesive energy (eV/atom)		2.51	2.23	
Heat of formation ΔH(eV/atom)		−0.451	−0.416	
Bulk modulus B (Mbar)		0.17	0.13	
$\partial B/\partial P$		4.0	3.7	
Nearest-neighbor distance $d_{K\text{-}Sb}=d_{K\text{-}K}$ (Å)		3.58	3.70	3.68

[a]Reference 58.

constraint of maintaining the space-group symmetry. In addition, for the calculation of the bulk modulus and to determine the variation of the crystal structure under pressure, a series of calculations at constant volume has been performed. Corrections for the Pulay stress are applied in calculating the pressure. The bulk modulus has been determined by fitting the energy-volume and pressure-volume data by a Murnaghan equation.[57]

III. THE OCTET COMPOUND K_3Sb

A. Atomic structure

K_3Sb crystallizes in the face-centered cubic (fcc) BiF_3 structure (space group $Fm\bar{3}m$) with 16 atoms per unit cell.[58] As for the pure alkali metal, the LDA underestimates the equilibrium atomic volume (see Table II), but the large negative excess volume of nearly 40% is correctly predicted. The gradient corrections lead to almost perfect agreement of the calculated lattice parameter with experiment, but hardly influence the excess quantities: volume and heat of formation are almost unchanged. The strong contraction on alloying is almost entirely due to a compression of the softer alkali atoms: compared to pure K, the K-K distances are reduced by 19.2% (from 4.58 Å to 3.70 Å). This corresponds to a reduction of the atomic volume of the K atoms by about 55%, i.e., only slightly larger than the negative excess volume per K atom of 52%. First-order perturbation theory accounting only for electrostatic effects and for an equilibration of the electronic pressure within the atomic spheres[15] predicts for K_3Sb an excess volume of $\sim$50%. Our present *ab initio* results confirm the correctness of the physical arguments behind the Zintl principle. The pronounced asymmetry of the compression is already a first hint to the strong ionic character of the octet compound. The bulk modulus calculated for the octet compound is about four times larger than that of pure K and more than two times lower than that of pure Sb. Again this confirms that the nature of the chemical bonding is entirely different from the metallic bond in K and the semimetallic character of Sb.

B. Electronic structure

Figure 1 shows the total, local, and angular-momentum decomposed electronic densities of states (DOS) of K_3Sb.

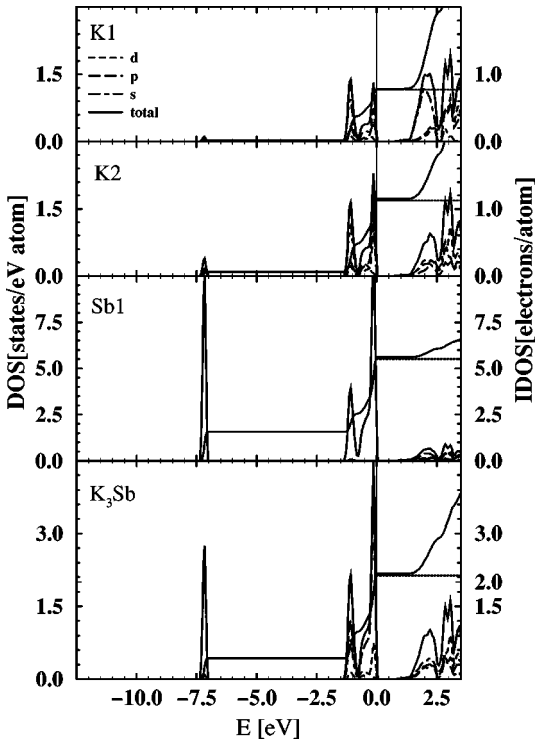

FIG. 1. Total, local, and angular-momentum decomposed electronic density of states (DOS) in K_3Sb with the BiF_3 structure. The right-hand scale shows the integrated density of states.

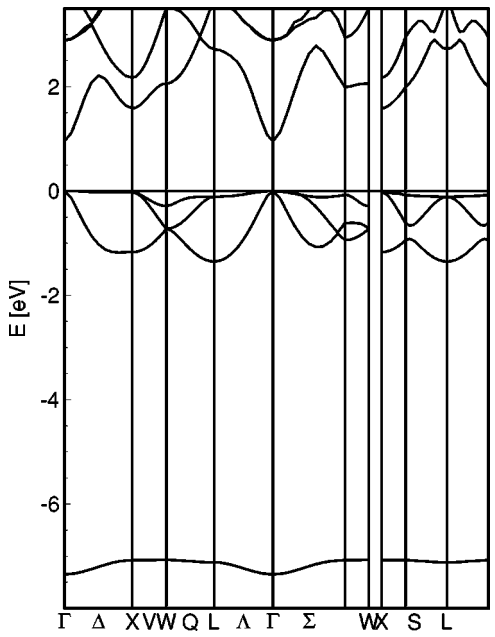

FIG. 2. Electronic band structure of K_3Sb along the principal symmetry lines.

The decomposition of the DOS has been performed by projecting the plane-wave components of the eigenstates onto spherical waves inside atomic spheres with the radii $R_K = 2.18$ Å and $R_{Sb} = 1.93$ Å; for further details see Ref. 59. The radii of the atomic spheres have been chosen in accordance with the arguments presented above: If the atomic volume of Sb is assumed to remain unchanged on alloying, a radius ratio of $R_K/R_{Sb} \simeq 1.13$ is calculated for the octet compound. Figure 2 presents the dispersion relations of the electronic eigenstates. In general, the electronic structure conforms with the results expected for the octet compound: the lowest valence band is a very narrow Sb *s*-band, the highest occupied band is a Sb *p* band. Although the local K DOS contributing to the band close to the Fermi level is by no means small (the integrated DOS reaches almost one electron per atom, so local charge neutrality is nearly exactly preserved), the strongly mixed angular-momentum character of the K DOS suggests that the states contributing to the DOS are in reality Sb states, overlapping into the K atomic spheres. The density of states on the two inequivalent K sites are also different. All atomic sites in the BiF_3 structure have body-centered-cubic symmetry with eight nearest neighbors at $d_1 = a\sqrt{3}/4$ and six next-nearest neighbors at $d_2 = a/2 \simeq 1.15 d_1$. The atoms at the K2 sites, placed in the tetrahedral holes of the fcc sublattice with four Sb and four K nearest neighbors give a larger contribution to the valence band than those on the K1 sites lying in the octahedral holes, with only six next-nearest Sb atoms.

The lowest conduction band is dominated by alkali states, again with a remarkable difference in the local K DOS: at the K1-sites the lowest peak has distinct *s* character, it is well separated from the rest of the conduction band. At the K2 sites the lowest peak has a stronger *p* character; an *s* peak appears at somewhat higher energies. The larger contribution of the local K2 DOS to the valence band together with the structure of the K2 conduction band suggests that there is some degree of covalent bonding between the Sb *p* states and *s*,*p* hybridized K2 states.

A further characteristic detail of the electronic structure is that the very high electronic pressure at the K sites (caused by the strong volume contraction) leads to a lowering of the 3*d* states relative to the 4*s* and 4*p* states with the result that above $\simeq$ 2.5 eV the conduction band shows appreciable *d* character.

K_3Sb is a narrow-gap semiconductor with a direct gap of 0.78 eV at the Γ point. The band originating from the lowest unoccupied eigenstate has a very strong dispersion (see Fig. 2) so that it makes only a very small contribution to the DOS. (In fact, the low-energy tail of the conduction band is almost invisible on the scale of Fig. 1.) The work of Tegze and Hafner[22] on a series of alkali-pnictide octet compounds has shown that such low-energy tails exist in the conduction bands of all BiF_3-type octet compounds except those formed by Li. There, owing to the small size of the Li ions the electrostatic potential is strong enough to push the Li *s* states far above the Fermi energy. In the Na-based compounds the Na *s* band crosses the Sb *p*-type valence band and this destabilizes the BiF_3 phase relative to the $AsNa_3$ structure.[22] In the alloys based on heavier alkali metals K, Rb, and Cs the *s* band is raised relative to the *d* band, leading to the stronger *d* character of the conduction band and again to a stable BiF_3 phase.

Altogether, our present pseudopotential-based electronic structure is in good agreement with the linear-muffin-tin-orbital (LMTO) calculations of Tegze and Hafner.[22] Some smaller differences (affecting mainly the more delocalized conduction-band states) arise from the muffin-tin form of the potential and the use of the atomic-sphere approximation in the LMTO calculations. The largest difference concerns the lowest unoccupied K *s* state at Γ and the highest occupied Sb *p* state at the *X* point: the LMTO predicts an indirect $X \rightarrow \Gamma$ gap of 0.40 eV, whereas we find a direct gap of 0.78 eV at Γ. We believe that the difference arises from the limited accuracy of the atomic-sphere approximation.

C. Analysis of chemical bonding

For the octet compound, the analysis of the local partial DOS already yields a fairly clear picture of the iono-covalent bond. This analysis may be corroborated by the calculation of the valence charge densities and the electron localization functions (ELF's). The ELF introduced by Becke and Edgecombe[60,61] is a convenient way to quantify the degree of localization of electrons. The definition of ELF is based on the fact that for a given ground-state density $\rho_0(\mathbf{r})$ the local kinetic energy $T_b(\mathbf{r})$ of a system of noninteracting bosons constitutes a lower bound to the local kinetic energy $T_f(\mathbf{r})$ of a system of fermions with the same density.[62] The electron localization function is then defined as

$$E(\mathbf{r}) = \frac{T_h(\mathbf{r})}{T(\mathbf{r}) + T_h(\mathbf{r})}, \tag{1}$$

where $T_h(\mathbf{r}) = \frac{3}{5}(\hbar^2/2m)(3\pi^2)^{2/3}\rho_0^{5/3}$ is the kinetic energy density of a noninteracting homogeneous electron gas of the density $\rho_0 = \rho(\mathbf{r})$ and $T(\mathbf{r}) = T_f(\mathbf{r}) - T_b(\mathbf{r})$ is the excess Pauli kinetic energy of the electron system. In regions where the excess kinetic energy is low (e.g., because the region is occupied by a single electron or by a pair of electrons with opposite spins) ELF is close to its maximum value $E(\mathbf{r})$

=1. Lower values correspond to a delocalized character of the electronic eigenstates. However, it is important to emphasize that both the valence charge distributions and the localization functions are calculated on the basis of the pseudo-orbitals and hence do not reproduce the nodal structure of the true orbitals (see Refs. 42, 43, and 45 for the description of the valence states within the ultrasoft pseudopotential scheme).

For the octet compound both the charge-density distribution and the electron-localization functions confirm the ionic character of the compound: Isosurfaces (see Fig. 3 for the ELF surfaces) form almost ideal spheres around the Sb sites, demonstrating the localization of the valence electrons in saturated s^2p^6 octets.

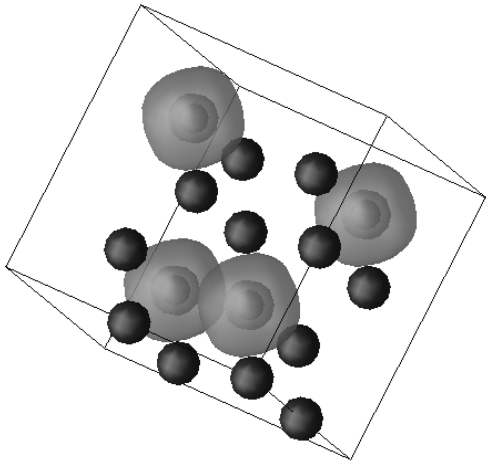

FIG. 3. Isosurfaces of the electron-localization function ELF in K_3Sb with $E(\mathbf{r})=0.82$. Small light spheres are Sb atoms, larger dark spheres are K atoms. The light frame indicates the unit cell.

IV. EQUIATOMIC CLUSTER COMPOUND

A. Atomic structure

The equiatomic compounds of the lighter pnictide elements (P, As, Sb) with the alkali metals form complex crystal structures with characteristic helical chains of the pnictide atoms. KSb and NaSb crystallize in the monoclinic LiAs structure[9] while RbSb and CsSb assume the orthorhombic NaP structure.[63] Despite the difference in symmetry the local coordination is very similar in both structures: The Sb atoms are arranged in infinite spiral chains parallel to the *b* axis with bond angles varying between 109° and 114°; the intrachain distances are rather close to the shortest interatomic distances in pure Sb. The alkali atoms may also be considered to be arranged in spirals coaxial with the Sb helices, rotated about 180° and with larger spiral radius. However, the spiral arrangement of the K atoms does not reflect a characteristic property of the K-K chemical bond. The main role of the alkali atoms is to isolate neighboring Sb helices from each other. So their spiral structure is merely a consequence of a space-filling arrangement.

TABLE III. Structural and cohesive properties of monoclinic (LiAs-type) KSb, calculated in the local-density approximation. Experimental values (after Ref. 58) are given in parentheses.

Pearson symbol $mP16$, space group $P2_1/c$				
Atomic positions within the unit cell				
		x	y	z
K1	(4*e*)	0.21922 (0.2189)	0.39867 (0.3990)	0.33180 (0.3318)
K2	(4*e*)	0.23921 (0.2395)	0.66687 (0.6668)	0.03151 (0.0312)
Sb1	(4*e*)	0.32111 (0.3222)	0.89883 (0.8991)	0.28704 (0.2876)
Sb2	(4*e*)	0.31676 (0.3191)	0.16633 (0.1662)	0.12152 (0.1199)
Lattice parameters				
$a=7.0724(7.156)$ Å		$b=6.8793(6.916)$ Å $b/a=0.973(0.966)$	$c=13.2068(13.355)$ Å $c/a=1.867(1.866)$ Å	$\beta=115.20°(115.17°)$
Atomic volume		$\Omega=36.324\,(37.397)$ Å^3		
Excess volume		$\Delta\Omega=-24.11\,(-26.2)\%$		
Cohesive energy		$E=3.42$ eV/atom		
Heat of formation		$\Delta H=-0.436$ eV/atom		
Bulk modulus		$B=0.18$ Mbar $\partial B/\partial P=4.6$		
Interatomic distances				
$d_{K\text{-}K}=3.818,3.874,3.949(3.86,3.92,3.98)$ Å $d_{K\text{-}Sb}=3.457-3.753(3.51-3.82)$ Å $d_{Sb\text{-}Sb}=2.817,2.848(2.83,2.85)$ Å				
Bond angles along the Sb chains				
$\theta=109.1°,114.0°(109.4°,113.9°)$				

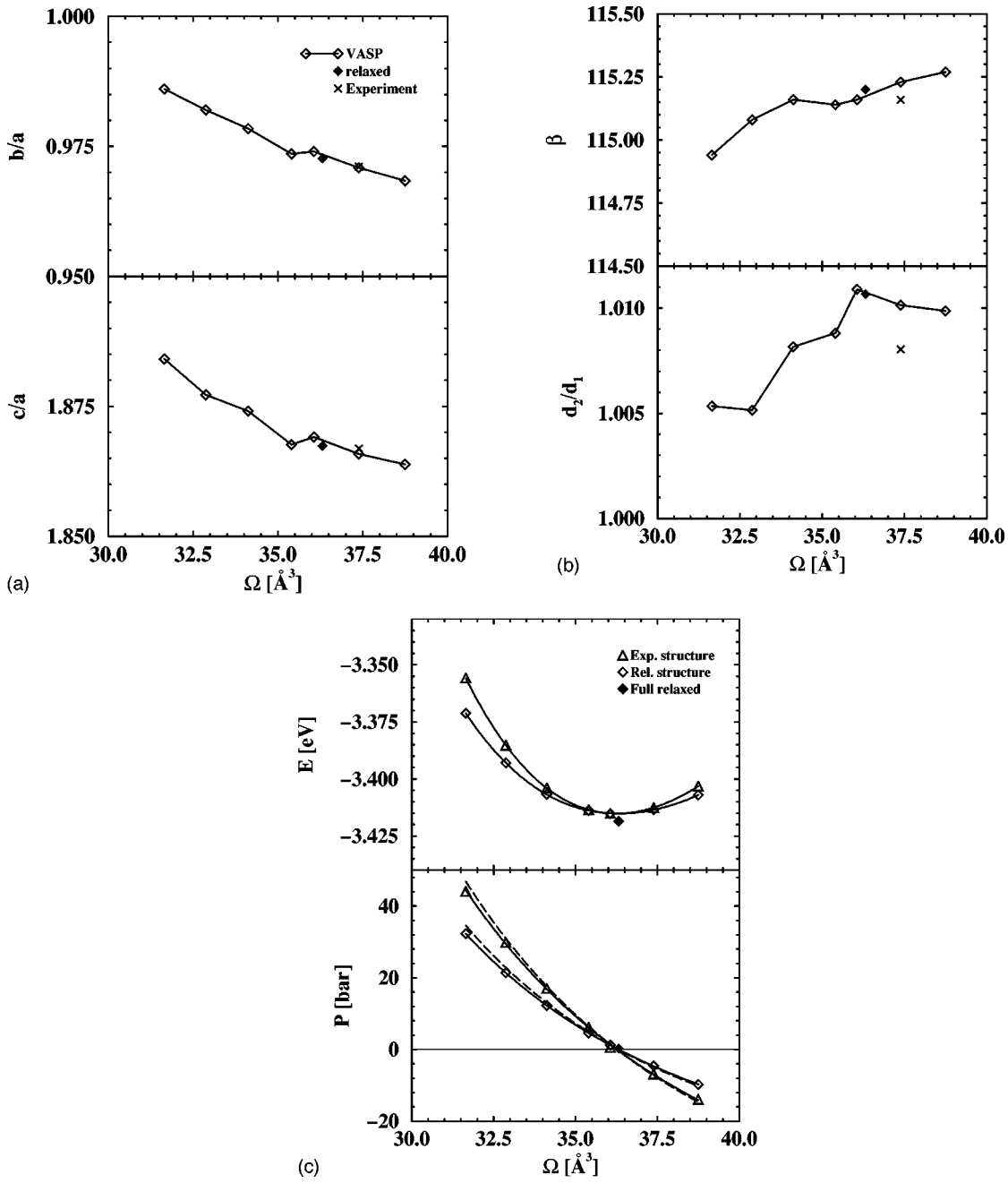

FIG. 4. (a) Variation of the axial ratios of monoclinic KSb with the atomic volume. (b) Variation of the ratio d_2/d_1 of long and short intrachain bond lengths and of the chain angles under compression. (c) Energy-volume and pressure-volume relationships calculated with fixed internal parameters (triangles) and with fully relaxed crystal structure (squares). Full and dashed curves in the lower panel represent the pressure calculated via differentiation of the $E(V)$ relation and via the virial theorem, respectively.

Except for the Sb spirals, the nearest-neighbor coordination is quite irregular. On average, each atom is surrounded by six atoms of the other kind, forming distorted octahedra plus about two atoms of the same kind (those forming the helices). This analysis of the structure suggests the following qualitative picture of the chemical bonding in KSb: The K atoms transfer the single valence electron to the Sb atom. The Sb^- ion is isoelectronic to the Te atom, and the helical Sb_∞^- chains are stabilized by Peierls-distorted $pp\sigma$ bonds like those in trigonal Te (see, e.g., Refs. 64, 65, and 48). In Te the Peierls distortion leads to trimerization of the p band into a $pp\sigma$ bonding, a nonbonding $pp\sigma°$ (''lone pair'') and a $pp\sigma^*$ antibonding band. The strength of the $pp\sigma$ bond determines the length of the intrachain bond, but the structure of the helix (bond and dihedral angles) is influenced by lone-pair interactions. In KSb and in the other monoantimonides the alkali atoms separate neighboring Sb_∞^- helices and suppress lone-pair interactions. Hence the structure of the spirals is largely determined by the Sb-K interactions. In trigonal Te, all bonds along the helices are equivalent, in monoclinic KSb the chains are dimerized: short and long bonds differing by 0.03 Å in length alternate along the helices. The dimerization may be considered as a consequence of a Jahn-Teller distortion of the symmetric arrangement. An interesting point is that alternating short and long bonds have also been found in isolated Te chains embedded in the cavi-

ties of a zeolite;[66] their bonding properties have been discussed by Ikawa and Fukutome.[67]

The LDA calculations underestimate the equilibrium atomic volume of KSb by about 2.8%, but otherwise predict the complex structure with surprisingly high accuracy (see Table III): The axial ratios of the monoclinic cell are accurate to 0.7% (b/a) and 0.5% (c/a); the error in the angle β is almost zero. The atomic positions within the unit cell are also reproduced with high accuracy: the degree of dimerization of the Sb-Sb bond lengths and of the bond angles along the helices is accurately predicted. The variation of axial ratios (b/a) and (c/a) and of the monocline angle β and the dimerization ratio d_2/d_1 with volume is shown in Fig. 4. The axial ratios slightly increase under compression; the dimerization decreases as expected as a consequence of the increased interchain interactions. Expansion of the volume on the other hand does not enhance the degree of dimerization.

The energy-volume and pressure-volume relations are shown in Fig. 4(c). We find that far from the equilibrium volume, the pressure-induced changes in the internal structural parameters have an important influence on the pressure-volume relations. Neglect of the internal relaxation would increase the bulk modulus from B=0.18 Mbar to 0.25 Mbar and its pressure derivative would be changed from $\partial B/\partial p = 4.6$ to 4.3.

The calculation predicts an excess volume of $\Delta\Omega = -24.11\%$, to be compared with a measured volume contraction of -26.2%. On the other hand, first-order perturbation theory predicts a contraction of $\sim 40\%$, i.e., nearly as large as for the octet phase. The importance of band-structure effects neglected in the lowest-order approximation is a signature of the increasing importance of covalent bonding effects. If we calculate the apparent atomic volume of K by subtracting the atomic volume of pure Sb from the equilibrium atomic volume of the compound, we find for both the octet and the polyanionic compounds almost the same value of $\tilde{\Omega}_K \sim 43$ Å^3 (we use the GGA result for K_3Sb and the LDA value for KSb to reduce the systematic density-functional error). This is a striking confirmation of the ''rule of constant additive volume increments'' proposed by Biltz and Weibke[68] many years ago.

B. Electronic structure

The calculated electronic structure of KSb (see Fig. 5 for the total and partial densities of state as well as for the integrated DOS, Fig. 6 for the dispersion relations) confirms the Zintl picture of the electronic and chemical bonding properties sketched above. The partial DOS has been calculated by projection onto spherical waves within spheres with radii $R_K = 2.28$ Å and $R_{Sb} = 1.95$ Å, chosen in accordance with the picture of compressed K spheres and a constant volume of the Sb spheres. The lowest valence band is a Sb s band whose form is characteristic for one-dimensional ($ss\sigma$) bonds. This band contains exactly two electrons per atom. The helical structure of the chain introduces a characteristic splitting of the s band into four parts (although the DOS minimum at ~ -10.0 eV is very weak—but see the dispersion relations). The s band shows a strong dispersion along the helical axes and almost none in the perpendicular directions.

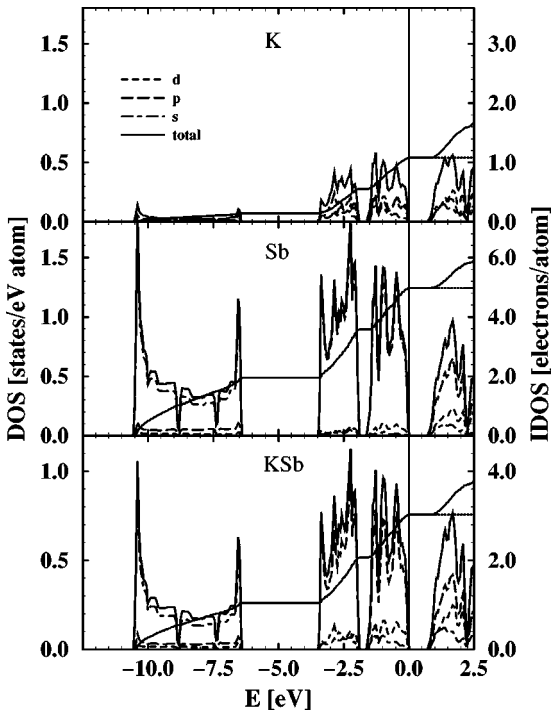

FIG. 5. Total, local, and angular-momentum decomposed differential and integrated electronic density of states in KSb with the monoclinic LiAs structure. The right-hand scale refers to the integrated density of states.

The bands around the Fermi level are a bonding, a nonbonding, and an antibonding Sb p band, separated by small gaps. The Fermi level falls into the larger nonbonding-antibonding gap. The smallest direct gap of $E_g \sim 0.70$ eV is found halfway along $\overline{\Gamma B}$. Indirect gaps of about the same width are found between the almost dispersionless valence states along Z-Γ-B and the lowest conduction-band state. As for the octet compound the local DOS on the K sites is nonnegligible: both the bonding and nonbonding Sb p bands contain about 1.5 electrons per atom on the Sb sites and 0.5 electrons per atom on the K sites. Hence the integration of the local charges indicates again a local charge neutrality. The important point is again that the local valence-band DOS on the K sites has strongly mixed angular momentum character, indicating that the ''K charges'' in reality arise from the overlapping tails of the Sb states.

As a consequence of the fourfold structure of the spiral Sb chains, each band is split into four subbands, with weak dispersion along the helical axes and overlapping only in the Γ-Y direction (see Fig. 6).

The antibonding $pp\sigma^*$ band overlaps with the lowest K band, which shows a strong d character; this again is a consequence of the large reduction of the volume of the K spheres. The overlap with the K-derived band leads to a stronger dispersion of the $pp\sigma^*$ bands along all symmetry directions.

As for the octet compound we note a reasonable agreement of the electronic structure with the LMTO results of Tegze and Hafner[22] (these where, however, only calculated for the experimentally determined structure.).

C. Analysis of the chemical bonding

Our interpretation of the electronic structure receives a striking confirmation by the analysis of the partial valence

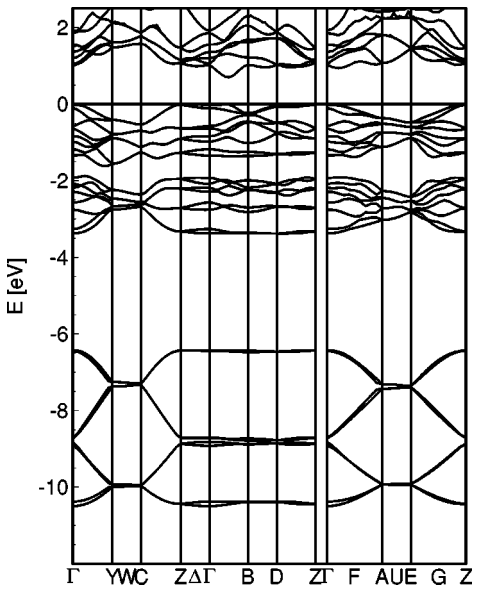

FIG. 6. Electronic band structure of monoclinic KSb along the principal symmetry lines.

charge distributions and the electron localization functions. Figure 7 shows isosurfaces of the partial electron density calculated for three occupied valence bands and the lowest empty conduction band. The $ss\sigma$ band extending from -10.5 eV to -6.5 eV is characterized by almost spherical charge distributions centered at the Sb sites, extending a bit farther along the chain links. The bonding $pp\sigma$ band (-3.5 to -2.0 eV) shows characteristic bond charges, located halfway between the Sb atoms (remember that we plot pseudo-charge-densities—hence the ''holes'' at the Sb sites). The nonbonding $pp\sigma°$ band shows dumbbell-shaped charge densities, centered at the Sb sites and oriented perpendicular to the intrachain bonds—these are precisely the ''lone-pair'' electrons. The antibonding $pp\sigma*$ band has a charge distribution that is evidently based on the same local orbitals than the bonding $pp\sigma$ states, but now out of phase on neighboring Sb-sites. Clearly no charges centered at the K sites can be identified.

This is also confirmed by the electron localization function (Fig. 8). The most strongly localized valence electrons evidently belong to the spin-saturated lone-pair states, with a weaker degree of localization for the bonding $pp\sigma$ states. We also see that the part of the valence-charge distribution extending closest to the K sites stems from the lone-pair states [see also Fig. 7(c)]. The strong localization of precisely these states justifies the assignment made above.

V. K-ENRICHED CLUSTER COMPOUNDS: K_5Sb_4

The phase diagrams of the binary systems of Sb with the heavier alkali metals K, Rb, and Cs are characterized by a series of compounds intermediate between the 3:1 octet compounds and the 1:1 polyanionic cluster compounds. The stoichiometry ranges between 5:2 and 5:4 (see, e.g., Villars and Calvert[58]). Similar compounds, e.g., a K_4P_3 phase, have also been identified in the alkali-enriched phosphorus and alkali-arsenic systems.[69] Among the alkali-enriched antimonides, only the crystal structure of K_5Sb_4 (isotypic to Rb_5Sb_4 and

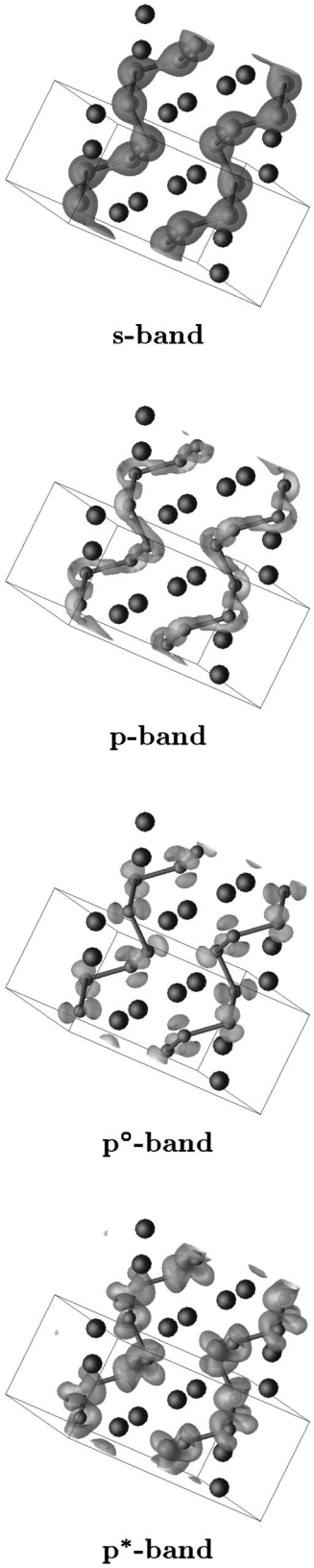

FIG. 7. Isosurfaces of the partial valence-charge distributions of the $ss\sigma$, $pp\sigma$, $pp\sigma°$, and the $pp\sigma*$ bands of KSb. Large balls represent the K atoms, smaller balls the Sb atoms (with nearest-neighbor bonds visualized by connecting bars). The light frame indicates the monoclinic unit cell. Compare text for details.

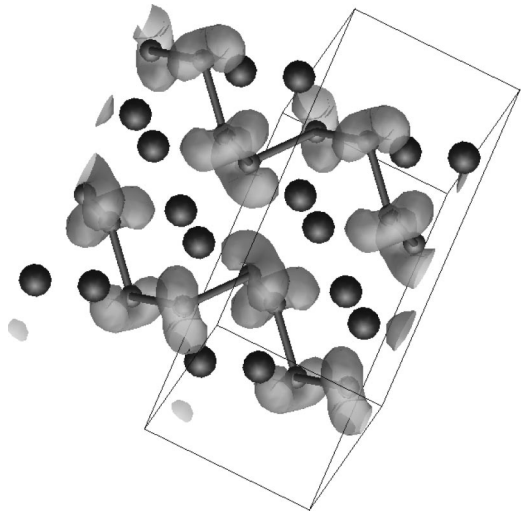

FIG. 8. Isosurfaces of the electron localization function $E(\mathbf{r})=0.75$ of the occupied states in KSb. Cf. text.

Rb_5As_4) has been determined in detail.[69,35] In general, the crystal structures of these compounds are characterized by short chains of pnictide atoms with interatomic distances close to those in the pure elements and wide bond angles. Again the crystal structures have tentatively been interpreted in terms of radical polyanions (P_3^{4-} or Sb_4^{5-}) stabilized by strong covalent bonds. However, as dangling bonds at the chain ends remain at least partially unsaturated, the electronic character of these compounds remains poorly understood.

A. Atomic structure

K_5Sb_4 crystallizes in a monoclinic structure with two formula units per cell. Each Sb atom lies in a center of a trigonal K_6 prism. Four prisms condense via the rectangular faces such that the centering Sb atoms form short zigzag chains. Neighboring four-prism units share an acute edge of the terminal prism such as to form a two-dimensional corrugated layered framework. Neighboring layers are displaced by half of the height of a K_6 prism, such that each K atom capes the rectangular face of the neighboring prism. Altogether the terminal Sb atoms of the Sb_4 chains are coordinated by 8 K plus 1 Sb and the bridging Sb atoms by 7 K plus 2 Sb. It has been proposed[69,35] that the Sb_4 units should be considered as Sb_4^{5-} polyanions in the spirit of the Zintl principle, with partially occupied antibonding states.[69]

In the context of the present study the compound K_5Sb_4 is of interest as being intermediate between the saltlike octet compound and the polyanionic compound KSb having saturated covalent bonds in the polyanions.

Table IV summarizes the LDA results for the structural and cohesive properties. The LDA error in the equilibrium volume is -4.2%, i.e., intermediate between the error for the octet compound and that one of the polyanionic cluster compound. As the LDA contraction affects all cell parameters likewise, all characteristic features of the crystal structure are

TABLE IV. Structural and cohesive properties of K_5Sb_4, calculated in the local-density approximation. Experimental values (after Ref. 69) are given in parentheses.

Pearson symbol $mP18$, space group $C2/m$				
Atomic positions within the unit cell				
		x	y	z
K1	($4i$)	0.1017 (0.1023)	0 (0)	0.3922 (0.3926)
K2	($4i$)	0.7535 (0.7538)	0 (0)	0.1651 (0.1659)
K3	($2a$)	0 (0)	0 (0)	0 (0)
Sb1	($4i$)	0.45606 (0.45604)	0 (0)	0.17456 (0.17612)
Sb2	($4i$)	0.39330 (0.39496)	0 (0)	0.39049 (0.39078)
Lattice parameters				
$a=12.1230(12.316)$ Å		$b=5.4023(5.491)$ Å	$c=11.10732(11.258)$ Å	$\beta=112.07°(112.25°)$
		$b/a=0.446(0.446)$	$c/a=0.916(0.914)$ Å	
Atomic volume		$\Omega=37.487$ (39.148) Å^3		
Excess volume		$\Delta\Omega=-24.94$ (-22.29)%		
Cohesive energy		$E=3.21$ eV/atom		
Heat of formation		$\Delta H=-0.438$ eV/atom		
Bulk modulus		$B=0.18$ Mbar		
		$\partial B/\partial P=4.5$		
Interatomic distances				
$d_{K\text{-}K}=3.987-4.060(4.079-4.112)$ Å				
$d_{K\text{-}Sb}=3.480-3.693(3.546-3.738)$ Å				
$d_{Sb\text{-}Sb}=2.774,2.812(2.790,2.815)$ Å				
Bond angle along the Sb chains				
$\theta=106.69°(107.26°)$				

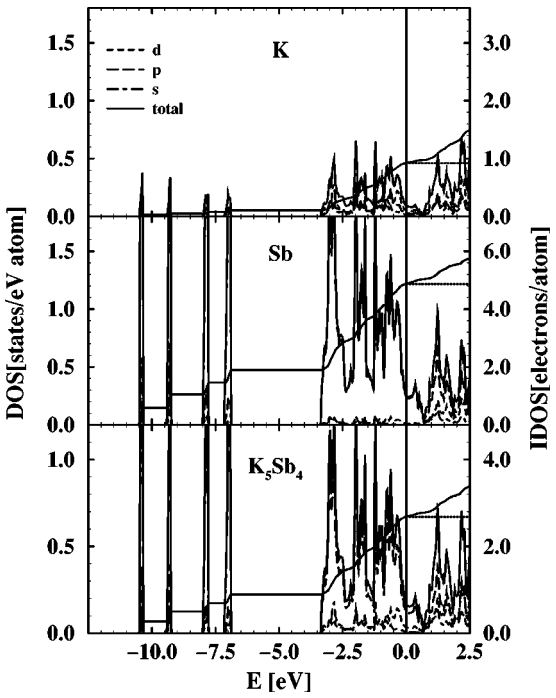

FIG. 9. Total, partial, and angular-momentum decomposed differential and integrated density of states of K_5Sb_4. The right-hand scale refers to the integrated density of states (thin lines).

nevertheless predicted with high accuracy. This concerns in particular the structure of the Sb_4 chains with slightly shorter Sb-Sb bond lengths for the terminal than for the bridging atoms and a decreased bond angle compared to the KSb phase.

The cohesive energy of K_5Sb_4 is within numerical accuracy equal to the compositionally averaged cohesive energies of K_3Sb and KSb. This correlates rather well with the observation[69] that K_5Sb_4 is only marginally stable and tends to disproportionate into KSb and K.

B. Electronic structure and chemical bonding

The electronic structure and chemical bonding properties of K_5Sb_4 have been analyzed in terms of the electronic dispersion relations, the total and partial local densities of state, and the partial valence charges. For comparison we have also calculated the molecular eigenstates of an isolated Sb_4 cluster with the same geometry as the Sb_4 units in the intermetallic compound.

Figure 9 shows the total and partial electronic density of states of K_5Sb_4. The partial densities of state have been calculated in terms of the projection of the plane-wave components of the eigenstates onto spherical waves, assuming a radii of $R_K = 2.25$ Å and $R_{Sb} = 1.93$ Å for K and Sb spheres, respectively. Figure 10 shows for comparison the molecular eigenvalues of the Sb_4 cluster (the energy scales have been matched at the bottom of the valence bands).

The lowest group of eigenstates, below -6.5 eV, consists of the molecular *s* orbitals of the Sb_4 units. The partial valence charge densities of eigenstates 1 to 4 of the cluster (see Fig. 11) and of the four lowest groups of bands of the crystal (see Fig. 12) display distinct $ss\sigma$ character.

States with binding energies between -3.5 eV and the deep DOS minimum close to 2.5 eV contain six electrons per

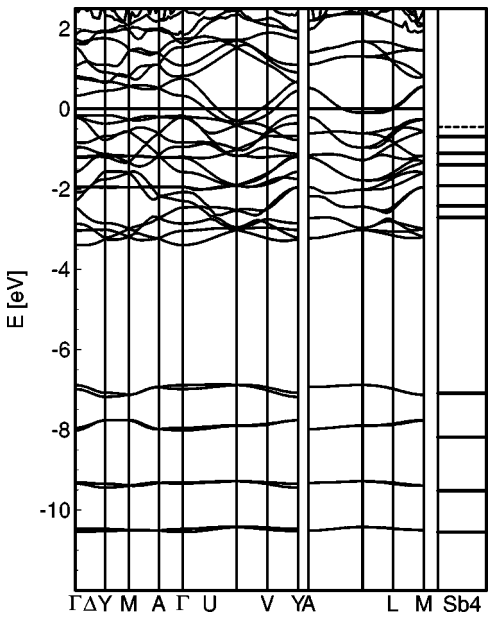

FIG. 10. Electronic band structure of monoclinic K_5Sb_4 along the principal symmetry lines. The side panel shows the molecular eigenstates of an isolated Sb_4 cluster. Energy scales are matched at the bottom of the bands.

Sb atom; these are bands mostly derived from the Sb *p* states. The following band (not shown in Fig. 9) is dominated by K states with a mixed *s* and *d* character. However, compared to the equiatomic KSb compound we note a stronger overlap of the highest Sb states and the lowest K states

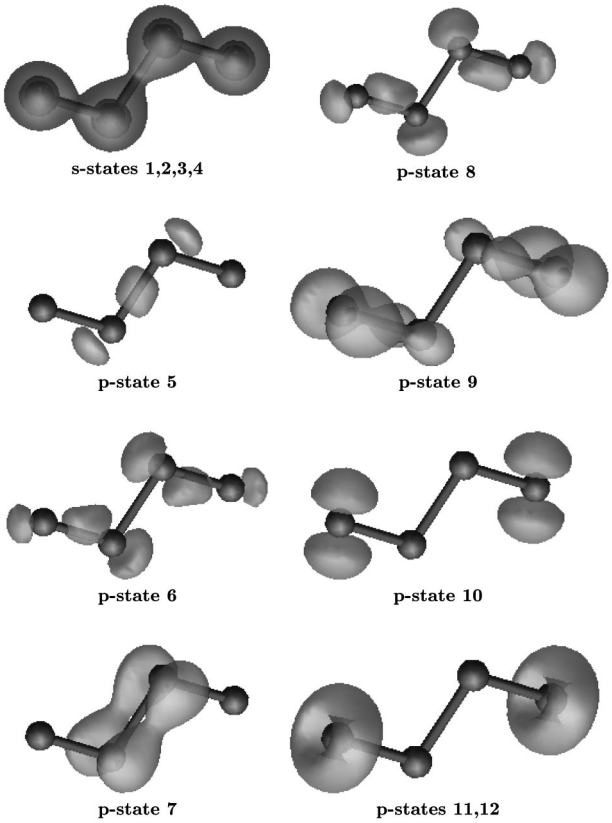

FIG. 11. Isosurfaces of the partial valence-charge distributions in the isolated Sb_4 cluster.

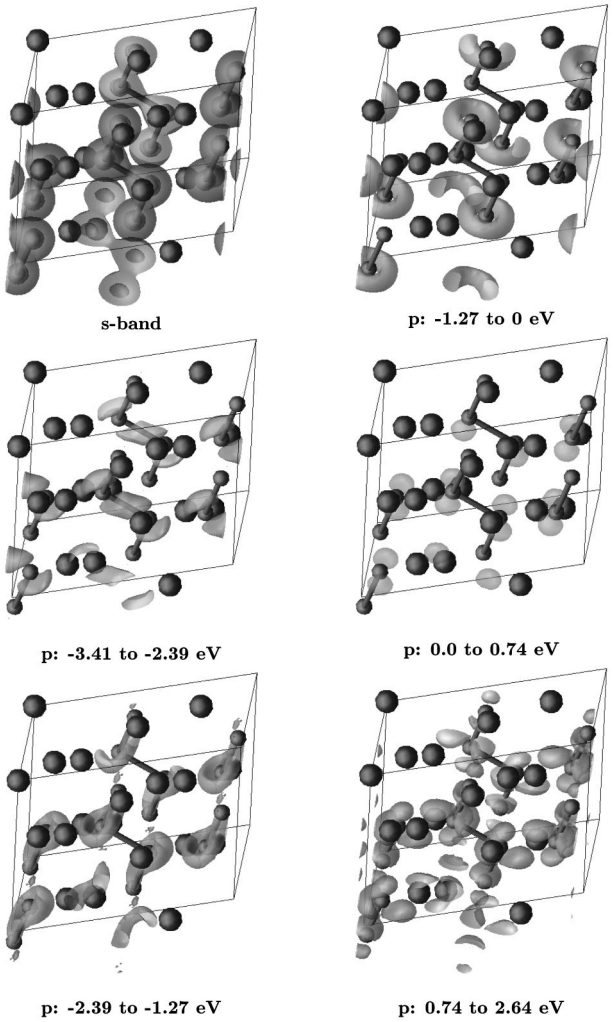

FIG. 12. Isosurfaces of the partial valence-charge distributions in K_5Sb_4. Large balls represent K atoms, smaller ones Sb atoms, next neighbors connected via bars. The light frame indicates the monoclinic unit cell. Cf. text.

(both empty). The Sb band complex displays a different structure than in KSb, because the Sb atoms are now arranged in flat zigzag units and not in three-dimensional helical chains. The tripartite structure of the occupied part of the valence band corresponds roughly to the three doublets of occupied eigenstates in the free Sb_4 cluster. The deep minimum in the DOS at $E=0.74$ eV corresponds to a band filling where the bonding $pp\sigma$ states within the chains, the lone-pair states at the central Sb atoms, and the dangling bonds at the chain ends are occupied.

The valence-charge distributions displayed in Fig. 11 allow the following characterization of the molecular eigenstates of Sb_4. (a) States 1 to 4 are $ss\sigma$ bonding. (b) Eigenstates 5 and 6 are $pp\sigma$ bonding in the bridging bond and in the terminal bonds of the cluster, respectively. (c) State 7 describes a $pp\pi$ bridging bond. (d) State 8 is again a $pp\sigma$ at the terminal bonds, (e) state 9 is $pp\pi$ bonding at the same bonds (with a slightly larger weight at the terminal sites). (f) States 10 to 12 contain nonbonding p states at the terminal atoms, directed normal to the bonds. These states have dangling-bond character.

In the crystalline intermetallic compound K_5Sb_4 the lowest group of Sb p bands (extending from -3.41 to -2.39 eV) contains states of $pp\sigma$ character on the central ''bridging'' bond of the polyanion (see Fig. 12). The second group of bonds (from -2.39 eV to -1.27 eV) is formed by p states on the two central Sb atoms oriented normal to the bridging bonds, but also with some bonding character on the terminal bonds. These states have no immediate counterpart among the eigenstates of the isolated cluster. The highest group of occupied valence states (extending from -1.27 eV to the Fermi level) is dominated by nonbonding, dangling-bond-like p states at the terminal Sb atoms, oriented normal to the bonds. States immediately above the Fermi energy up to the pronounced DOS minimum at 0.74 eV are nonbonding p states at the central Sb atoms. Finally the topmost empty Sb p states (between 0.74 eV and 2.64 eV) have antibonding character at the terminal Sb bonds, but also show charge extending towards the K sites—this reflects the K/Sb mixing in this energy range.

Hence this analysis shows that although the structure of the valence band is undoubtedly determined by the strong attractive potential of the Sb_4^{-5} polyanions, it differs in many important details from the molecular eigenstates of an isolated Sb_4 cluster. The differences are due to the electrostatic potential of the K^+ ions, the charging of the polyanions, and intercluster and K-Sb interactions.

VI. DISCUSSION AND CONCLUSIONS

We have presented detailed local-density-functional calculations of K-Sb intermetallic compounds ranging from the composition of the octet phase K_3Sb to the equiatomic phase KSb and included the intermediate phase K_5Sb_4 characterized by Somer *et al.*[35] We find that whereas generalized gradient corrections are necessary for an accurate prediction of the equilibrium atomic volume and the bulk modulus of pure K and of the K-rich compound, their importance decreases with increasing Sb content. However, we note that the volume and heat of formation of the compound are only marginally affected by the gradient corrections. At a fixed volume, the LDA and the GGA also lead to identical predictions for the details of the atomic and the electronic structures. Hence the effect of the GGA is essentially to contribute an isotropic pressure favoring expansion and reducing the cohesive energy.

For the compound K_3Sb we predict a negative excess volume of about 38% arising almost entirely from the compression of the K atoms. Although integration over the local charge distributions indicates that the atomic spheres centered around the K and Sb sites remain essentially charge neutral, the analysis of the electronic eigenstate confirms that the K_3Sb is properly considered as mainly ionic, as confirmed in a very striking way by the analysis of the electron localization function.

The LDA calculations lead to a very accurate prediction of the complex monoclinic structure of the KSb. At fixed atomic volume, the structure depends on 17 independent parameters—all have been optimized to find the energetically most favorable structure. Even details such as the weak dimerization of the Sb-Sb bond along the Sb_∞ helices are correctly predicted. The analysis of the electronic structure

of KSb confirms the validity of the Zintl picture: the occupied part of the valence band is described in terms of $ss\sigma$ and bonding and nonbonding $pp\sigma$ and $pp\sigma^{\circ}$ bonds, respectively; the lowest unoccupied band is just the antibonding $pp\sigma^{*}$ Sb band overlapping with the lowest K band. In accordance with this picture, the highest degree of electron localization is found for the spin-saturated lone-pair electrons forming $pp\sigma^{\circ}$ band.

We have also presented the first theoretical investigation of an alkali-pnictide compound with the stoichiometry intermediate between the saltlike octet and the equiatomic polyanionic phase. Again we find that the complex structure with the polyanions Sb_4^{-5} forming zigzag chains is correctly predicted within the LDA. The electronic structure is similar, but slightly more complex than for the equiatomic phase: The valence band consists of a group of almost dispersionless $ss\sigma$ states at high binding energy and $pp\sigma$ states around the Fermi level. However, due to the low symmetry of the Sb_4 units and the increased K-Sb interaction, their detailed analysis is more complex. In this connection it is interesting to point out that at a composition K_5Sb_4 only half of the dangling bonds of the Sb_4 unit can be saturated. A full saturation of these states would be possible at a composition K_3Sb_2. A compound at this composition has been found in the Cs-Sb (Bi) system, but so far the crystal structure could not be determined. For such a compound one would expect the pronounced DOS minimum we find also in K_5Sb_4 to be exactly at the Fermi level. Altogether we find that the $pp\sigma$ bonds stabilizing both the infinite helical chains in KSb and the small zigzag clusters in K_5Sb_4 have considerable flexibility. Hence we expect that the same bonding principle will also determine the local order above the melting point. Results of detailed *ab initio* molecular-dynamics studies are reported in the following paper.[70]

ACKNOWLEDGMENTS

This work was supported under project No. P10445-PHY by the Austrian Science Funds within the European Cooperation on the field of Scientific and Technical Research (COST), Action D6 (Project ''Chemical Processes and Reactions under Extreme or Non-Classical Conditions'').

[1] *Chemistry Structure and Bonding of Zintl Phases and Ions*, edited by S. Kanzlarich (Verlag Chemie, Weinheim, 1996).
[2] E. Zintl and G. Brauer, Z. Phys. Chem. Abt. *B* **20**, 241 (1933).
[3] E. Zintl, J. Goubeau, and W. Dullenkopf, Z. Phys. Chem. Abt. A **154**, 1 (1931).
[4] W. Hückel, *Structural Chemistry of Inorganic Compounds* (Elsevier, Amsterdam, 1951), Vol. II, p. 83.
[5] P. Böttcher, Angew. Chem. Int. Ed. Engl. **27**, 759 (1986).
[6] P. Böttcher and R. Keller, Z. Anorg. Allg. Chem. **90**, 731 (1986).
[7] M. L. Saboungi, J. Fortner, J. W. Richardson, A. Petric, M. Doyle, and J. E. Enderby, J. Non-Cryst. Solids **156-158**, 356 (1993).
[8] D. Cromer, Acta Crystallogr. **12**, 41 (1959).
[9] E. Busmann and S. Lohmeyer, Z. Anorg. Allg. Chem. **312**, 53 (1961).
[10] H. G. von Schnering and W. Hönle, Z. Anorg. Allg. Chem. **456**, 194 (1979).
[11] W. Müller and K. Volk, Z. Naturforsch. B **32**, 709 (1977); **33**, 275 (1978).
[12] T. Asada, T. Jarlborg, and A. J. Freeman, Phys. Rev. B **24**, 510 (1981); **24**, 857 (1981).
[13] D. Ellis, G. Benesh, and E. Byron, Phys. Rev. B **16**, 3308 (1977).
[14] A. Zunger, Phys. Rev. B **17**, 2582 (1978).
[15] J. Hafner and W. Weber, Phys. Rev. B **33**, 747 (1986).
[16] N. Christensen, Phys. Rev. B **32**, 207 (1985).
[17] J. Hafner and W. Jank, Phys. Rev. B **44**, 11 662 (1991).
[18] F. Springelkamp, R. A. de Groot, W. Geertsma, W. van der Lugt, and F. M. Mueller, Phys. Rev. B **32**, 2319 (1985).
[19] M. Tegze and J. Hafner, Phys. Rev. B **39**, 8263 (1989).
[20] M. Tegze and J. Hafner, Phys. Rev. B **40**, 9841 (1989).
[21] J. Robertson, Adv. Phys. **32**, 361 (1983).
[22] M. Tegze and J. Hafner, J. Phys.: Condens. Matter **3**, 2449 (1992).
[23] M. Cohen and J. Chelikowsky, *Electronic Structure and Optical Properties of Semiconductors* (Springer, Berlin, 1988).
[24] G. Kresse, J. Furthmüller, and J. Hafner, Phys. Rev. B **50**, 13 181 (1994).
[25] D. L. Price, M. L. Saboungi, H. T. J. Reijers, G. Kearley, and R. White, Phys. Rev. Lett. **66**, 1894 (1991); D. L. Price, M. L. Saboungi, and W. S. Howells, Phys. Rev. B **51**, 14 923 (1995).
[26] J. Richardson, D. Price, and M. Saboungi, Phys. Rev. Lett. **76**, 1852 (1996).
[27] W. van der Lugt, J. Phys.: Condens. Matter **8**, 6115 (1996).
[28] R. Winter, in *Thermodynamics of Alloy Formation*, edited by Y. Chang and F. Sommer (The Minerals, Metals and Materials Society, London, 1997).
[29] R. Stolz, R. Winter, W. Howells, and R. McGreevy, J. Phys.: Condens. Matter **3**, 577 (1995).
[30] J. Hafner, J. Phys.: Condens. Matter **1**, 1133 (1989).
[31] G. Galli and M. Parrinello, J. Chem. Phys. **95**, 7505 (1991).
[32] G. de Wijs, G. Pastore, A. Selloni, and W. van der Lugt, Phys. Rev. B **48**, 13 459 (1993).
[33] G. de Wijs, G. Pastore, A. Selloni, and W. van der Lugt, Europhys. Lett. **27**, 667 (1994).
[34] G. de Wijs, G. Pastore, A. Selloni, and W. van der Lugt, J. Chem. Phys. **103**, 5031 (1995).
[35] M. Somer, M. Hartweg, K. Peters, and H. von Schnering, Z. Kristallogr. **195**, 103 (1991).
[36] J. Bernard and W. Freyland, J. Non-Cryst. Solids **205-207**, 62 (1996).
[37] M. Saboungi, J. Ellefson, G. Johnson, and W. Freyland, J. Chem. Phys. **88**, 5812 (1988).
[38] H. Redslob, G. Sternleitner, and W. Freyland, Z. Naturforsch. A **27A**, 587 (1982).
[39] C. Bergman, K. Seifert-Lorenz, M. V. Coulet, R. Céolin, R. Bellissent, and J. Hafner, Europhys. Lett. **43**, 539 (1998).
[40] P. Lamparter, W. Martin, and S. Steeb, Z. Naturforsch. A **38A**, 329 (1983).
[41] P. Lamparter, W. Martin, S. Steeb, and W. Freyland, J. Non-Cryst. Solids **61+62**, 279 (1984).
[42] G. Kresse and J. Hafner, Phys. Rev. B **47**, 558 (1993).

[43] G. Kresse and J. Hafner, Phys. Rev. B **49**, 14 251 (1994).
[44] G. Kresse and J. Furthmüller, Phys. Rev. B **54**, 11 169 (1996).
[45] G. Kresse and J. Furthmüller, Comput. Mater. Sci. **6**, 15 (1996).
[46] J. Perdew and A. Zunger, Phys. Rev. B **23**, 5048 (1981).
[47] D. Vanderbilt, Phys. Rev. B **41**, 7892 (1990).
[48] G. Kresse and J. Hafner, J. Phys.: Condens. Matter **6**, 8245 (1994).
[49] K. Seifert, J. Hafner, J. Furthmüller, and G. Kresse, J. Phys.: Condens. Matter **7**, 3683 (1995).
[50] K. Seifert, J. Hafner, and G. Kresse, J. Non-Cryst. Solids **205-207**, 624 (1996).
[51] J. Perdew and Y. Wang, Phys. Rev. B **33**, 8822 (1986).
[52] J. Perdew, Phys. Rev. B **33**, 8822 (1986).
[53] A. Becke, Phys. Rev. A **38**, 3098 (1988).
[54] J. Perdew, J. A. Chevary, S. H. Vosko, K. A. Jackson, M. R. Pederson, D. J. Singh, and C. Fiolhais, Phys. Rev. B **46**, 6671 (1992).
[55] H. J. Monkhorst and J. D. Pack, Phys. Rev. B **13**, 5188 (1976).
[56] M. Methfessel and A. T. Paxton, Phys. Rev. B **40**, 3616 (1989).
[57] D. C. Wallace, *Thermodynamics of Crystals* (Wiley, New York, 1972), p. 50.
[58] P. Villars and N. Calvert, *Pearson's Handbook of Crystallographic Data for Intermetallic Phases* (American Society for Metals, Metals Park, OH, 1990).
[59] A. Eichler, J. Hafner, J. Furthmüller, and G. Kresse, Surf. Sci. **346**, 300 (1996).
[60] A. Becke and K. Edgecombe, J. Chem. Phys. **92**, 5397 (1990).
[61] B. Silvi and A. Savin, Nature (London) **371**, 683 (1994).
[62] Y. Tal and R. Bader, Int. J. Quantum Chem., Symp. **12**, 153 (1987).
[63] H. G. von Schnering, W. Hönle, and G. Krogull, Z. Naturforsch. B **34**, 1678 (1979).
[64] P. Littlewood, Crit. Rev. Solid State Mater. Sci. **11**, 229 (1983).
[65] P. Littlewood, J. Phys. C **13**, 4855 (1983); **13**, 4875 (1983).
[66] Y. Katayama, M. Yao, Y. Ajiro, M. Inui, and H. Endo, J. Phys. Soc. Jpn. **58**, 1811 (1989).
[67] A. Ikawa and H. Fukutome, J. Phys. Soc. Jpn. **59**, 1002 (1990); **59**, 4041 (1990).
[68] W. Biltz and F. Weibke, Z. Anorg. Allg. Chem. **223**, 321 (1935).
[69] W. Hönle, M. Hartweg, U. Hartweg, and H. von Schnering, Z. Kristallogr. **186**, 131 (1989).
[70] K. Seifert-Lorenz and J. Hafner, following paper, Phys. Rev. B **59**, 843 (1999).